IAC-22.LBA.C1.2
DESIGN AND STUDY OF SATELLITE CONSTELLATIONS IN FROZEN LOW LUNAR ORBITS

Sergey Trofimov
Keldysh Institute of Applied Mathematics, RAS, Russian Federation, trofimov@keldysh.ru

Maksim Shirobokov
Keldysh Institute of Applied Mathematics, RAS, Russian Federation, shirobokov@keldysh.ru
Mikhail Ovchinnikov
Keldysh Institute of Applied Mathematics, RAS, Russian Federation, ovchinni@keldysh.ru

The research paper studies the potential of frozen low lunar orbits to be used in the design of constellations for global and regional communication/navigation. We introduce a novel two-stage approach to the robust lunar frozen orbit design based on two non-gradient techniques, the Bayesian optimization and the Nelder-Mead algorithm. The developed methodology allows revealing orbits with the eccentricity vector periodic behavior over the one-year propagation interval in the full dynamical model. By leveraging the convenient nomogram with basic constellation visibility parameters and lower bound coverage curves, several Walker-type low-altitude configurations are identified and properly adjusted to be frozen. The frozenness condition appears to be achievable without changing the orientation of orbital planes. Visibility and coverage metrics (multiplicity of continuous coverage for specified sites, polar regions, or the whole surface; position dilution of precision) of candidate constellations are analyzed. Several promising designs of frozen constellations in near-circular low orbits are singled out. The frozen orbit stability and station-keeping cost are discussed.

I. INTRODUCTION

The steadily growing worldwide interest in lunar exploration and numerous plans to establish a lunar base encourage the study and development of multi-spacecraft constellations around the Moon for communication and navigation purposes. A low-altitude constellation of cheap small spacecraft that provides low signal latency and is well suited for both optical and laser short-range intersatellite links, would be a very attractive option. However, pursuing that way, one should deal with the two key problems. The first problem is the efficient constellation deployment. In contrast to the case of Earth-orbiting constellations, the multiple-launch deployment scheme implying at least one dedicated launch followed by a high-energy transfer for each of the orbital planes, appears to be prohibitively expensive when dealing with large distributed systems around the Moon. Therefore, most of the researchers have been so far focused primarily on constellations in high lunar orbits [1,2] and even more distant libration point orbits [3,4], with much lower number of spacecraft and less costly launches. A promising solution that potentially allows one not to abandon the use of low lunar orbits (LLOs) seems to be in leveraging a ballistic lunar transfer (BLT), a special kind of low-energy lunar transfers exploiting the solar gravitational perturbation. In the course of a very long BLT, several groups of spacecraft can be successively separated from a mothership by a small impulse and then captured into orbits with different right ascension of the ascending node values [5].

The second problem to be solved in order a small satellite lunar constellation to be feasible is to select long-term stable orbits that uniformly surround the Moon. Its irregular gravity field substantially limits the range of suitable lunar orbits—especially of low altitude—with a reasonable lifetime. Due to the fact that traditional approaches developed for the design of Earth constellations were not aimed at exploiting complex natural dynamics in the circumlunar space, they require much propellant to reject gravitational perturbations. For example, the operational lifetime of the lunar constellation made of 3U CubeSats with a standard monopropellant thruster does not exceed 100 days [6]. The only viable solution is represented by frozen orbits, a special class of orbits with nearly constant mean values of the eccentricity vector components, $e_x = e\cos\omega$ and $e_y = e\sin\omega$. Here e is the eccentricity and ω is the argument of periapsis. The Earth's gravity is a dominant source of perturbation in high lunar orbits, whereas in LLOs, the condition of frozenness is fully dictated by the Moon's gravity. Medium lunar orbits experience both effects.

The present paper further develops and expands the study of frozen orbit constellations begun in [7].

A two-stage non-gradient optimization procedure is devised to search for frozen LLOs. At the first stage, a coarse global minimum search for eccentricity vector periodic behavior over the one-year time interval is done by the robust Bayesian optimizer augmented with the sequential domain reduction. After that, at the second stage, the solution found is fine-tuned by the Nelder-Mead method. Such an approach is quite flexible; it permitted us to design lunar frozen orbits so that their orbital elements meet user-defined box constraints. A useful nomogram with basic visibility parameters and lower bound global coverage curves, first presented below, was successfully employed for the assessment whether a given constellation design is suitable for communication or navigation needs. If so, a set of frozen orbits as much close to those from the considered design as possible, is generated; their coverage and stability characteristics are evaluated.

The paper has the following structure. The next chapter introduces the dynamical model used in the study, including a simple approximation rule of how to truncate the lunar gravitational potential in case of propagating low or medium orbits. Chapter III is devoted to the non-gradient optimization procedure and its implementation details. Then, the constellation performance metrics monitored in this research are summarized in Chapter IV. The analysis of some candidate frozen constellations and the discussion of their performance, globally and in polar regions, are contained in Chapter V. Long-term stability issues for frozen LLOs are also commented there; the cost and optimal periodicity of orbital correction maneuvers are estimated.

II. DYNAMICAL MODEL

When dealing with the numerical propagation of lunar orbits, two major perturbation sources are the Moon's gravity and the Earth's gravity. In altitudes up to 2000 km, the former dominates over the latter (Fig. 1). The lunar gravitational potential is known to be complex. It is of great importance to properly truncate it in order to avoid excessive computations while retaining high propagation accuracy. Perhaps, the most systematic way to truncate the perturbing acceleration stems from the philosophy of perturbation theory: the truncated terms magnitude relative to the central (Newtonian) part of the gravitational acceleration should be bounded by some predefined small parameter ε. In our previous work [7], we have conducted a thorough examination of the maximum magnitude of gravitational acceleration imparted by spherical harmonics of various degree and order as a function of the orbital altitude. Based on the results of those numerical experiments, we proposed simple approximating expressions for the maximum degree and order of harmonics to be retained in the gravity field model. In this research, the $\varepsilon = 10^{-6}$ threshold is used, and the sufficiently accurate $N \times N$ model of lunar gravitational potential corresponds to

$$N = \left\lceil (25/h)^{0.8} \right\rceil$$

with altitude h measured in thousands km. The half square brackets in this formula denote, as usual, the ceiling function. As can be seen from Fig. 2, such an approximation is very accurate for low and medium lunar orbits up to 3000 km.

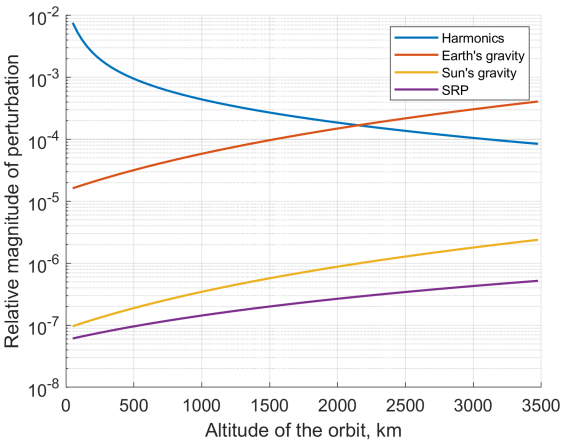

Fig. 1: Relative magnitude of perturbations as a function of the orbital altitude.

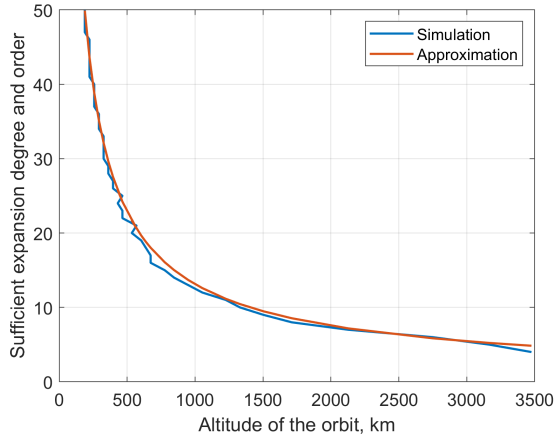

Fig. 2: Degree and order for the lunar potential expansion sufficient to ensure the truncated perturbing acceleration threshold $\varepsilon = 10^{-6}$.

Apart from the Moon, the Earth and the Sun are also taken into account as point gravitating sources. The positions of celestial bodies have been retrieved

from JPL's DE430 ephemeris model [8]. Finally, the solar radiation pressure effect is modeled. The area-to-mass ratio of 0.02 m^2/kg is assumed. Trajectories are propagated numerically using the variable-order Adams method (a Fortran routine similar to `ode113` routine in MATLAB) in rectangular Cartesian coordinates of the selenocentric celestial reference frame (SCRF), centered at the Moon's center of mass. The SCRF axes are parallel to those of the International Celestial Reference Frame [9].

III. DESIGN OF FROZEN ORBITS

The concept of a frozen orbit, an orbit with constant average eccentricity and argument of periapsis values, was first introduced for near-Earth orbits at the dawn of the space era and has soon become associated with an equilibrium of the averaged or doubly averaged system [10]. Unlike the Earth or an Earth-like oblate planet, the Moon has an irregular gravity field with no single dominant harmonic. Asymptotic expansions of the lunar orbiter perturbation theory, mostly derived in simplified models with low-degree harmonics and third-body attraction [11–13], fail to represent an accurate approximation to low-altitude frozen orbits, whereas more realistic models require tedious and lengthy symbolic computations [14,15]. Not surprisingly, mission designers prefer numerical techniques since they are much easier to understand and implement. Along with the brute-force search in the high-precision dynamical model [16,17], smarter approaches are also developed that are based on the numerical continuation of periodic orbit families via different predictor-corrector schemes [18,19]. At the same time, it is worth noticing that the condition of periodicity in the synodic frame, which is equivalent to having a repeating ground track [19], is formally a stronger condition than the frozenness because the latter assumes periodic behavior for the argument of periapsis and the eccentricity only, not imposing the constraint of synodic resonance on the altitude. It is therefore essential to build a more flexible technique of lunar frozen orbit design, capable of searching for long-lived orbits under user-specified constraints on their orbital elements. The equal spacing of circular near-polar constellation orbits around the Moon is a relevant example of such a constraint.

The major obstacle towards the robust design of frozen LLOs is very high sensitivity when an initial-guess orbit is propagated for a long time interval. It deteriorates the local correction procedure by a gradient method. So, we came up with a natural idea of using non-gradient methods. The best performance, among both gradient and non-gradient optimization solvers, is demonstrated by the Bayesian algorithm, one of the most powerful non-gradient techniques of optimizing a function that is computationally costly to evaluate [20]. In the earlier paper [7], MATLAB's `bayesopt` function was exploited. Currently, we use the improved Python version of the algorithm based on the open-source code developed by Nogueira [21]. This global optimization solver augmented with the sequential domain reduction tool allows speeding up the convergence process by adaptively squeezing the search domain. Another source of computational efficiency is due to translating such low-level routines as numerical integration to Fortran and then calling them by the `F2PY` wrapper from the NumPy library.

Now it is time to give the technical details of the posed optimization problem. The objective function is defined as the Euclidean norm of the difference in the eccentricity vector over the propagation interval

$$\sqrt{(\Delta e_x)^2 + (\Delta e_y)^2} \to \min$$

where $\Delta e_x = e_{x,f} - e_{x,0}$ and $\Delta e_y = e_{y,f} - e_{y,0}$ stand for the difference between the initial and final values of the eccentricity vector components. To search for Walker-type frozen constellations of a given altitude $h = h_{\text{ref}}$, we impose the box constraints

$$a_0 \in [a_{\min}, a_{\max}]$$
$$e_{x,0} \in [-e_{\max}, e_{\max}]$$
$$e_{y,0} \in [-e_{\max}, e_{\max}]$$

on the optimized vector $\boldsymbol{\xi} = (a_0,\, e_{x,0},\, e_{y,0})$, with the bounds being set to $e_{\max} = 0.02$ for the eccentricity and

$$a_{\min} = R_M + h_{\text{ref}} \cdot 0.95$$
$$a_{\max} = R_M + h_{\text{ref}} \cdot 1.05$$

for the semimajor axis. Here $R_M = 1737.4$ km is the mean radius of the Moon.

The initial values of the inclination and the right ascension of the ascending node can be set fixed: we found that they do not affect the iterative procedure convergence. The choice of right ascension values, as well as of the reference altitude, comprises the issue of preliminary constellation design, which is covered in the next chapter. What concerns the inclination, it is assumed to be $i_0 = 84°$ for all the orbital planes in any design considered. Such a value is close to one of the four inclinations at which frozen LLOs can be near-circular [15]. Suitable for observing lunar polar regions, the $i_0 = 84°$ inclination is at the same time more safe: strictly polar ($i = 90°$) constellations are more susceptible to the danger of collisions between the constellation satellites at high latitudes.

For definiteness, a spacecraft is assumed to start orbiting from the ascending node and the initial moment of time t_0 corresponds to the midnight of 1 Jan 2022. The propagation interval can be as long as one year (further, we considered $t_f = t_0 + 365$ days). The obvious initial guess $a_0 = R_M + h_{\text{ref}}$, $e_{x,0} = e_{y,0} = 0$ appeared to be adequate in all the cases.

The sequential domain reduction option was applied as follows. Starting with the 20th iteration, the search box size is multiplied by 0.95. The total number of Bayesian algorithm iterations is manually set to 130, which is enough for deep capture in the basin of attraction of a correct local minimum. After that, to further decrease the objective function value to as low as 10^{-4} and less, the Nelder-Mead non-gradient solver from the SciPy library is advised to be started from the point the Bayesian solver stopped with the same box constraints. The stopping condition of the Nelder-Mead solver was defined in terms of the optimized vector tolerance: $|\Delta\boldsymbol{\xi}| < \texttt{xatol} = 10^{-5}$.

To validate the suggested two-stage procedure of frozen orbit design, we performed a lot of numerical experiments for various orbital plane orientations in space and different reference altitudes. Particularly, we have reproduced two repeat ground track orbits (RGT) from the paper of Russell and Lara [19]. The eccentricity vector evolution for two RGTs, medium ($h \approx 3308$ km) and low ($h \approx 124$ km), drawn in that paper (reprinted for convenience in Figs. 3a and 4a), very closely matches (almost coincides) with what is observed in our simulations (see Fig. 3b and Fig. 4b, respectively).

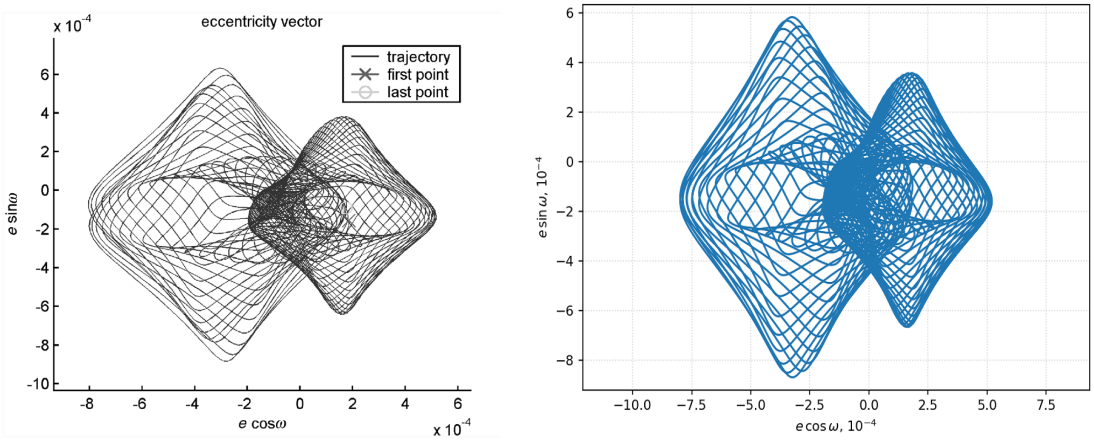

(a) retrieved from [19] (b) reproduced

Fig. 3: Eccentricity vector evolution for the 73-cycle RGT periodic orbit from [19].

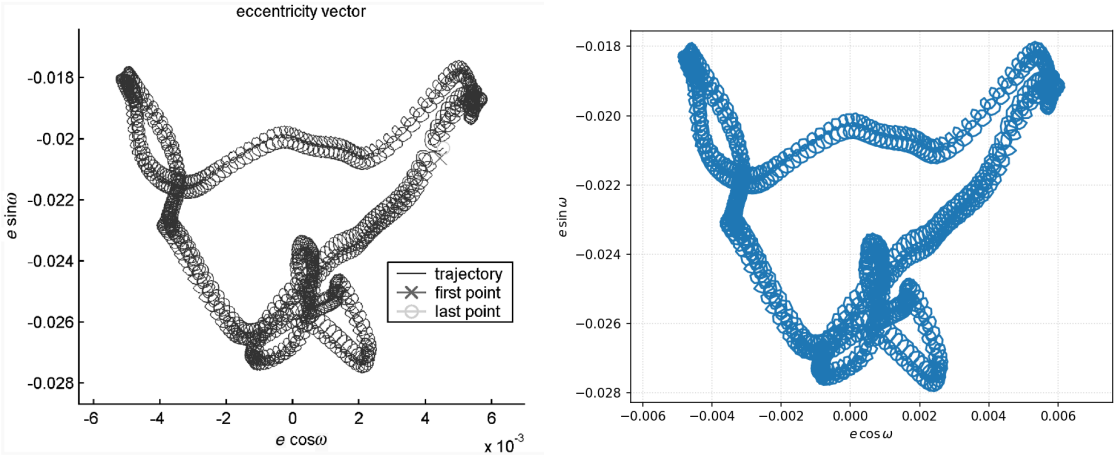

(a) retrieved from [19] (b) reproduced

Fig. 4: Eccentricity vector evolution for the 328-cycle RGT periodic orbit from [19].

Once a set of frozen orbits uniformly distributed around the Moon is obtained, initial states for same-plane satellites in a constellation may be assigned as states along the reference frozen orbit equidistant in time over the nominal orbital period.

A remark should be made that the lunar orbiter elements are usually given with respect to the mean-Earth/mean-rotation (MER) reference frame which is employed to define the selenographic coordinates. At the same time, the spherical harmonic expansion of the selenopotential is given with respect to the so called Principal Axes (PA) reference frame. Its axes are very close to those of MER. The rotation matrix for the MER–PA transformation can be found in [8]. As for the PA–SCRF transformation, its matrix can be constructed using lunar libration angles included in the ephemeris information.

IV. CONSTELLATION DESIGN AND PERFORMANCE METRICS

The preliminary step in the design of frozen LLO constellations is to select an orbital configuration we subsequently attempt to make frozen. In this study, we restrict ourselves to Walker–Mozhaev symmetric constellations in identical circular orbits distributed uniformly around the Moon. Four parameters are to be defined for such a constellation:

1) N, the total number of satellites;
2) P, the number of orbital planes;
3) h_{ref}, the reference altitude of all the planes;
4) the phase shift between the respective satellites in adjacent planes.

The phase shift for a Walker–Mozhaev constellation is usually characterized by integer F: it is expressed through this integer as $F\cdot 360^\circ/N$. Below we use the standard notation i°: $N/P/F$. Specifically, constellations 84°: $N/P/1$ are of our interest.

The design of symmetric constellations in identical circular orbits uniformly distributed around the spherical celestial body has been widely studied in a large number of papers since the pioneering works of Walker [22] and Mozhaev [23,24]. If a satellite orbits the body of radius R at altitude h, it covers the spot with the central half-angle φ (referred to as the footprint size in the below text) such that

$$\cos\beta = \frac{R+h}{R}\sin\frac{\alpha}{2} = \frac{R+h}{R}\cos(\varphi+\beta)$$

where β is the minimum elevation angle at which an orbiting satellite is still considered visible (Fig. 5).

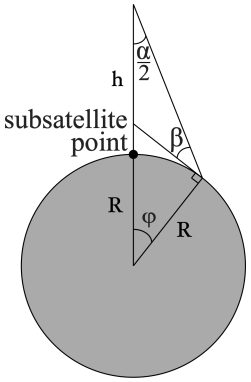

Fig. 5: Relation between the minimum elevation angle, the orbital altitude, and the footprint size.

Taking the value of $\beta = 5^\circ$ typically adopted for atmosphereless bodies such as the Moon, we have

$$\frac{h}{R} = \frac{\cos 5^\circ}{\cos(\varphi^\circ + 5^\circ)} - 1$$

This gives a one-to-one correspondence between the orbital altitude and the footprint size.

The other quantities uniquely determined by the footprint size are the lower bound for the number of orbital planes

$$P_{\min} = \left\lceil \frac{180^\circ}{2\varphi^\circ} \right\rceil$$

and the minimum number of satellites in each plane

$$(N/P)_{\min} = \left\lceil \frac{360^\circ}{2\varphi^\circ} \right\rceil$$

required for one-fold global continuous coverage. As for the total number of satellites in a single-coverage constellation, its static estimate from below

$$N_{1f} = 2 + \frac{60^\circ}{60^\circ - \arctan\sqrt{3}\cos\varphi}$$

is derived in the classical paper of Ballard [25]. Note that a simpler, but very close estimate

$$N_{1f} \approx P_{\min}\cdot(N/P)_{\min} = 162\cdot\left\lceil\left(\frac{10^\circ}{\varphi^\circ}\right)^2\right\rceil$$

can also be used. The lower bound estimate for four-fold global continuous coverage by Walker–Mozhaev constellations is much harder to get analytically. To the best of our knowledge, it has not been published yet. The simplified estimate

$$N_{4f} = 4\cdot N_{1f}$$

derived for street-of-coverage constellations is therefore utilized, despite such an estimate being slightly conservative for Walker–Mozhaev constellations.

In order to compactly and conveniently visualize the principal design parameters, we put forward the idea of a single nomogram, with the x-axis being the footprint size and the y-axis unified for the properly normalized four parameters (see Fig. 6):

- Orbital altitude, expressed in body's radii
- Free-space path loss (FSPL) of the signal power, normalized to its value at the altitude of $h = R$; it grows proportionally to the square of altitude
- Minimum number of satellites in a constellation to provide 1-fold coverage (in hundreds)
- Minimum number of satellites in a constellation to provide 4-fold coverage (in hundreds)

Moreover, the green color shades of the background stripes indicate the corresponding number of orbital planes at least required, starting with two planes for the rightmost stripe.

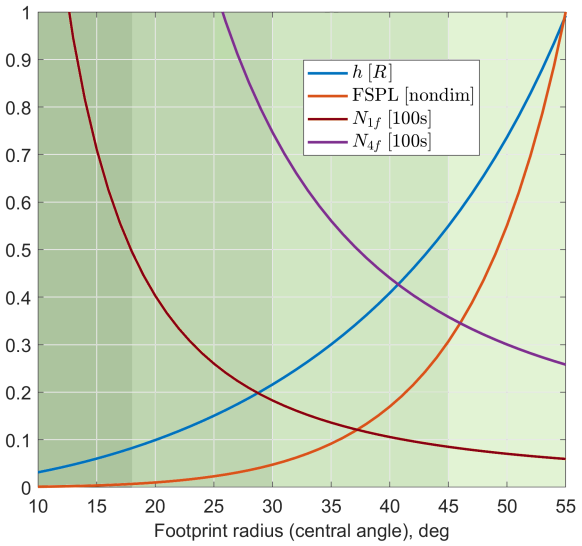

Fig. 6: Nomogram for basic coverage parameters as a function of the footprint size: the altitude of orbits, in R (blue); the free-space path loss (red) normalized to its value at $h = R$; the theoretical minimum constellation size, in 100s of satellites, for 1-fold (maroon) and 4-fold (violet) coverage. The 5 deg minimum elevation angle is assumed.

The advantage of the developed nomogram is its universality (i.e., validity for any particular celestial body) and comprehensiveness, which makes it quite convenient for the preliminary constellation design.

Leveraging the nomogram, we have selected two footprint sizes, $\varphi = 25°$ and $\varphi = 35°$, corresponding to the altitude values $h_{\text{ref}} = 0.15\, R_M \approx 261$ km and $h_{\text{ref}} = 0.3\, R_M \approx 522$ km, as potentially appropriate for candidate low-altitude lunar constellations: they ensure the total number of satellites does not exceed 100 even for navigation purposes. As for the number of orbital planes, our numerical analysis covers LLO constellations containing at least two orbital planes, no matter which of the two reference altitude values is taken.

Among the performance metrics tracked, we are most interested in median and minimum numbers of visible spacecraft, globally and in lunar polar zones, which we define as North and South polar caps with latitudes higher than 70°. Additionally, two craters, Boguslawsky (72.9 S, 43.2 E) and Manzinus (67.7 S, 26.8 E), were of specific interest to us as the primary and backup landing sites of Luna 25, the mission to the Moon Russia is scheduled to launch in late 2022. The constellation geometry quality for navigation is often quantified by the position dilution of precision (PDOP), a useful scalar metric that reflects how the user equivalent range error (UERE) is amplified due to poor configuration of visible satellites to result in higher user position uncertainty. The 50% (median) and 95% PDOP levels are tracked for both the poles and the craters of interest.

To evaluate the above mentioned metrics, we use a quasi-uniform grid on the Moon's surface which is generated as an outcome of the numerical optimization procedure similar to the one introduced in [26]. Specifically, to generate a grid of n almost uniformly distributed points on the unit sphere, one can search for unit vectors $\mathbf{r}_i \in \mathbb{R}^3$, $i = 1, \ldots, n$, that minimize the objective function

$$J = \sum_{1 \le i < j \le n} \log \frac{1}{|\mathbf{r}_i - \mathbf{r}_j|}$$

For convenience, the first six vectors $\mathbf{r}_1, \ldots, \mathbf{r}_6$ have been fixed to $(\pm 1, 0, 0)$, $(0, \pm 1, 0)$, and $(0, 0, \pm 1)$, the points on the MER frame axes, including North and South poles. Moreover, we fix $\mathbf{r}_7$ and $\mathbf{r}_8$ at positions of Boguslawsky and Manzinus craters. In this study, $n = 1200$ is set. Unlike our previous paper [7], where the optimization problem was solved by MATLAB's realization of the interior point algorithm, the trust-region interior point method from the Python SciPy library is exploited. The initial guess is generated as a three-dimensional Gaussian random vector of unit norm. The resulting grid is shown in Fig. 7.

V. CANDIDATE CONSTELLATIONS PERFORMANCE AND STABILITY

In the framework of this study, several dozens of LLO constellations have examined. All of them have successfully been made frozen by applying the novel

two-stage non-gradient technique. Among the whole set of different designs, we will focus further only on 5 configurations appeared to be best suited for some of the goals: global or local lunar surface coverage of a multiplicity high enough to ensure communication and navigation services. To visualize the parameters of the selected constellations, the five star marks are displayed on the introduced nomogram (see Fig. 8), with the y-value for each of the marks being equal to the total number of satellites (in 100s) and the label next to the mark designating the numbers of orbital planes and satellites per plane.

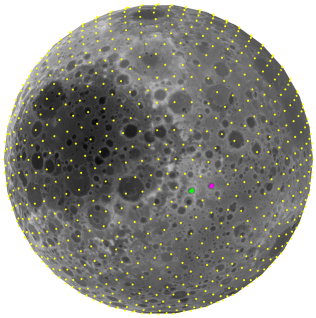

Fig. 7: Quasi-uniform surface grid of 1200 points with 8 sites included by default; among them are the North and South poles, as well as the craters Boguslawsky (light green) and Manzinus (purple).

Out of the five selected candidate constellations, three have an altitude of $h_{\text{ref}} = 261$ km, whereas the other two are designed for $h_{\text{ref}} = 522$ km. The major performance metrics of the candidate constellations are summarized in Table 1. Note that, in addition to earlier mentioned metrics, the minumum distance is also tracked between the satellites in a constellation since it is a very important safety parameter.

Based on the presented results, one can conclude that three constellations ($84°: 54/3/1$, $84°: 70/5/1$, $84°: 36/3/1$) are capable of providing navigation for the lunar polar zones, including the targeted craters and the poles themselves. Navigation quality is very good almost all the time. It is especially true for the $84°: 70/5/1$ constellation. Apart from high-precision polar navigation, it also provides the global communication service. The same property is shared by the $84°: 36/3/1$ constellation. Close performance can be attained with significantly smaller numbers of satellites and orbital planes, but at the cost of four times higher FSPL due to the doubled altitude. We should notice, however, that the larger the orbital altitude, the greater the minimum intersatellite distance. So, performance and safety vote for the altitude as high as the satellite power budget allows.

The one-year evolution of the eccentricity vector and the semimajor axis for each orbital plane of the three constellations is shown in Figs. 9–11. To avoid full overlapping, we displayed the curves for just one satellite in each orbital plane; the other satellites in the same plane have very similar evolution. It can be deduced from these figures that all the constellation orbits are indeed frozen and remain near-circular. A slight difference in the semimajor axis from plane to plane serves as the main instrument for meeting the frozenness condition.

If one seeks guaranteed navigation globally, over the entire lunar surface, the constellation size has to be significantly larger. Keeping a three-plane design of the 522 km constellation, the number of satellites in each plane needs to be increased almost threefold: the $84°: 99/3/1$ constellation is the first that attains global continuous coverage.

On the other part of the range, among the downsized constellations, the $84°: 18/2/1$ constellation at a 261 km altitude appears to be the most promising in case a continuous up/downlink for the lunar base in the polar region is required. There is no any other lunar constellation orbiting so low that is able to do such a thing more efficiently.

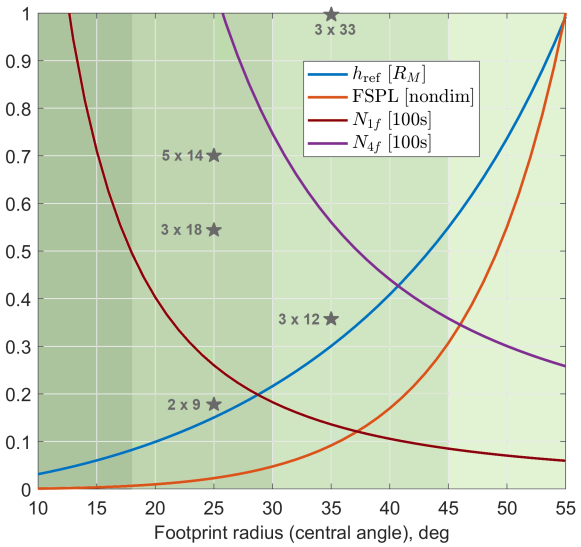

Fig. 8: Five candidate LLO constellations marked on the previously introduced nomogram.

We should remark that the conducted analysis is not in any sense an exhaustive search for those LLO constellations that can be made frozen for years and possess good performance metrics for lunar communication and navigation. The numerical results play an illustrative role to demonstrate opportunities the proposed powerful techniques and tools provide to a mission designer.

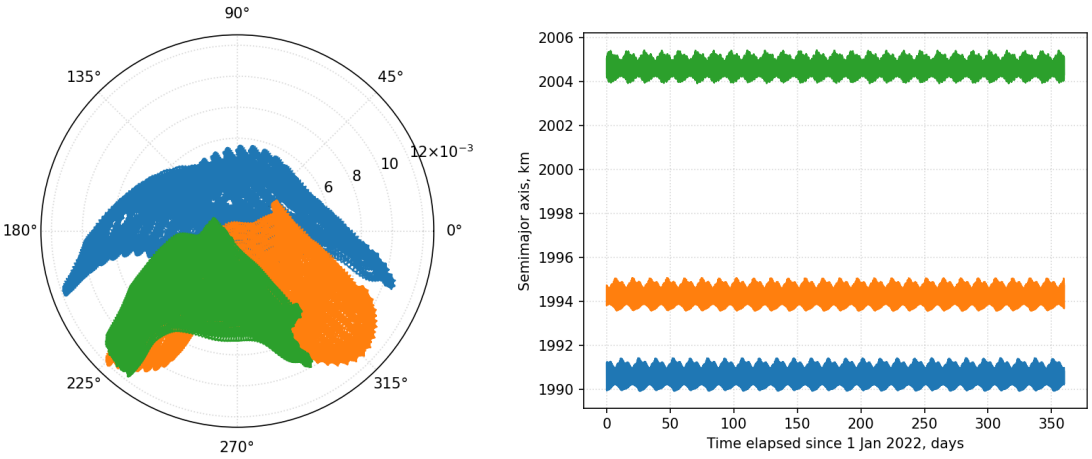

(a) eccentricity vector (b) semimajor axis

Fig. 9: One-year evolution of orbital elements for the 84°: 54/3/1 constellation ($h_{\text{ref}} = 261$ km).

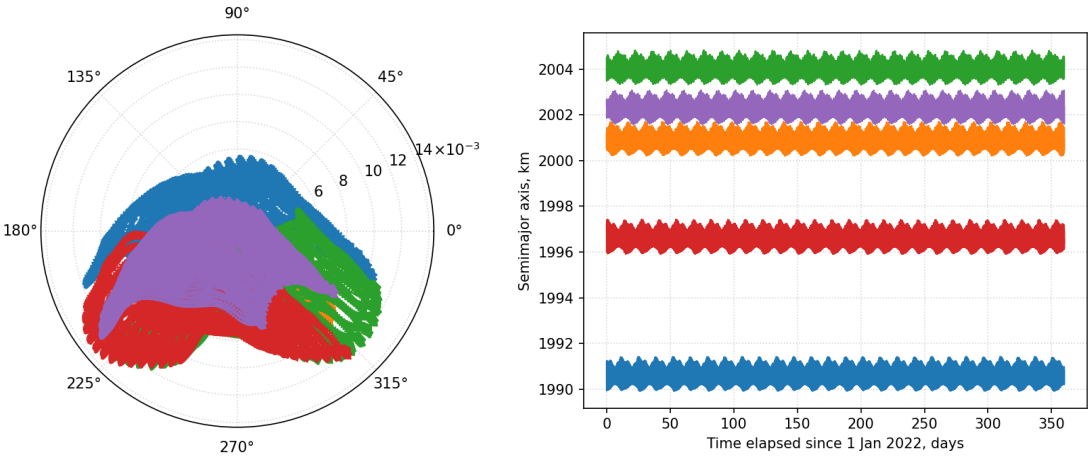

(a) eccentricity vector (b) semimajor axis

Fig. 10: One-year evolution of orbital elements for the 84°: 70/5/1 constellation ($h_{\text{ref}} = 261$ km).

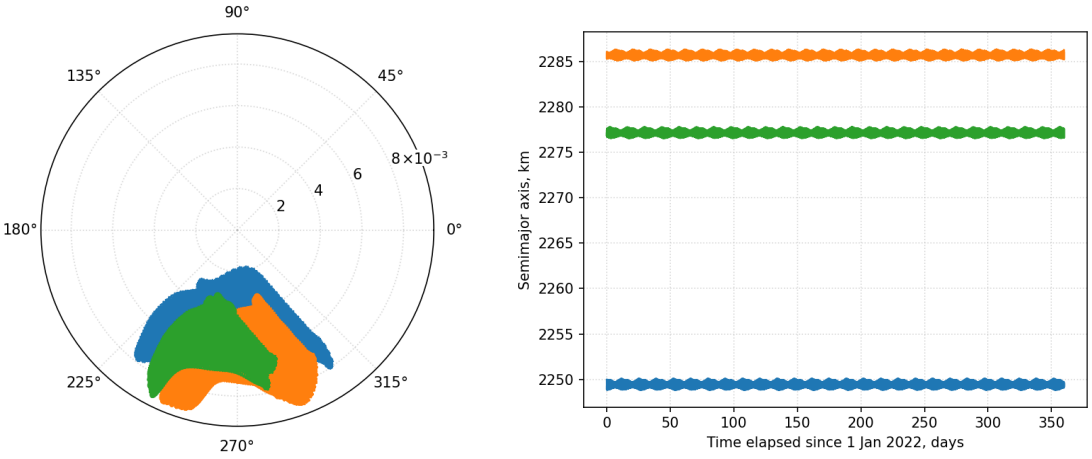

(a) eccentricity vector (b) semimajor axis

Fig. 11: One-year evolution of orbital elements for the 84°: 36/3/1 constellation ($h_{\text{ref}} = 522$ km).

Table 1: Coverage performance for some candidate constellations.

$h_{\text{ref}} = 261$ km	N_{global}	N_{North}	N_{South}	N_{Bogus}	$\text{PDOP}_{\text{Npole}}$	$\text{PDOP}_{\text{Spole}}$	$\text{PDOP}_{\text{Bogus}}$
84°: 18/2/1 $d_{\min} = 1.01$ km	min 0 med 0	min 1 med 2	min 1 med 2	min 1 med 2	N/A	N/A	N/A
84°: 54/3/1 $d_{\min} = 0.37$ km	min 0 med 2	min 4 med 7	min 4 med 6	min 4 med 6	95% 6.5 med 2.0	95% 6.9 med 2.1	95% 10.9 med 3.0
84°: 70/5/1 $d_{\min} = 0.54$ km	min 1 med 3	min 4 med 9	min 4 med 8	min 4 med 8	95% 3.2 med 1.9	95% 3.4 med 2.0	95% 4.8 med 2.4
$h_{\text{ref}} = 522$ km	N_{global}	N_{North}	N_{South}	N_{Bogus}	$\text{PDOP}_{\text{Npole}}$	$\text{PDOP}_{\text{Spole}}$	$\text{PDOP}_{\text{Bogus}}$
84°: 36/3/1 $d_{\min} = 2.66$ km	min 1 med 3	min 5 med 7	min 5 med 6	min 5 med 6	95% 7.2 med 1.8	95% 7.4 med 1.8	95% 8.2 med 2.3
84°: 99/3/1 $d_{\min} = 1.30$ km	min 4 med 7	min 16 med 19	min 15 med 18	min 16 med 18	95% 1.1 med 1.0	95% 1.1 med 1.0	95% 1.5 med 1.2

It was interesting to find that, though the frozen LLOs seem to be long-term stable, they are actually unstable, be it very mild instability. This fact can be proved based on the sign of the maximum Lyapunov characteristic exponent. More precisely, we estimate the leading finite-time Lyapunov exponent (FTLE)

$$\lambda\left(t;t_0\right) = \frac{\ln\|\mathbf{\Phi}(t;t_0)\|_2}{t-t_0}$$

by integrating the variational equations for the state transition matrix $\mathbf{\Phi}(t;t_0)$ alongside the equations of motion. When we increase the propagation interval, the leading FTLE tends to some limit value. For the frozen orbits with $h_{\text{ref}} = 261$ km, this value appears to be equal to $3.5\cdot10^{-4}$ and almost does not depend on a specific orbit. In the case of $h_{\text{ref}} = 522$ km, the result is similar: $3\cdot10^{-4}$. Converting to dimensional time units and inverting yields the characteristic instability time (Lyapunov time) of 1.1 to 1.3 months. According to numerous studies of spacecraft motion in the unstable dynamical environment, the optimal frequency of impulsive station-keeping burns [27] or optimal update time for low-thrust orbit control [28] can be estimated by the value of the instability time. It implies the optimal periodicity of frozen orbit corrections to be once per 1–2 months. The annual cost for a satellite to correct its orbit will supposedly not exceed 1–2% of the Delta-V budget allocated for the missions with extensive maneuvering between usual (non-frozen) LLOs: 150 m/s in the LRO mission [29] and the extended GRAIL mission [30] (note that the 5-month budget is indicated in the latter case). The future extension of this work will include the results of Monte-Carlo experiments to confirm feasibility of long-term station-keeping of frozen constellations.

VI. CONCLUSIONS

The whole toolkit of techniques and instruments has been presented for the easy and robust design of lunar frozen orbits of low altitude and constellations employing these orbits. The Bayesian/Nelder-Mead method of non-gradient optimization allows flexibly incorporating different design constraints and at the same time succeeds in satisfying the frozenness condition with high accuracy. The compact nomogram, specially developed here to visualize the preliminary design of Walker–Mozhaev constellations, has given useful insights regarding geometrical configurations capable of providing the lunar surface coverage. The numerical study of various constellation designs has revealed several promising configurations for the deployment of navigation infrastructure in polar zones also applicable to the task of global communication. The Lyapunov time estimated for all the considered orbits has shown mild instability, which may require negligible orbital corrections on a monthly basis.

VII. ACKNOWLEDGMENTS

The study was supported by the Russian Science Foundation (RSF) grant 19-11-00256.

REFERENCES

[1] Ely, T. A. and Lieb, E., "Constellations of Elliptical Inclined Lunar Orbits Providing Polar and Global Coverage," AAS/AIAA Astrodynamics Specialist Conference, Lake Tahoe, CA, August 7-11, 2005. Paper AAS 05-343, 18 p.

[2] Ely, T. A., "Stable Constellations of Frozen Elliptical Inclined Lunar Orbits," *The Journal of the Astronautical Sciences*, Vol. 53, No. 3, 2005, pp. 301–316.

[3] Xu, M., Wang, J., Liu, S., and Xu, S., "A New Constellation Configuration Scheme for Communicating Architecture in Cislunar Space," *Mathematical Problems in Engineering*, Vol. 2013. Article ID 864950, 14 p.

[4] Gao, Z.-Y. and Hou, X.-Y., "Coverage Analysis of Lunar Communication/Navigation Constellations Based on Halo Orbits and Distant Retrograde Orbits," *The Journal of Navigation*, Vol. 73, No. 4, 2020, pp. 932–952.

[5] Circi, C. and Teofilatto, P., "Weak Stability Boundary Trajectories for the Deployment of Lunar Spacecraft Constellations," *Celestial Mechanics and Dynamical Astronomy*, Vol. 95, No. 1–4, 2006, pp. 371–390.

[6] McManus, L. and Schaub, H., "Establishing a Formation of Small Satellites in a Lunar Flower Constellation," *The Journal of the Astronautical Sciences*, Vol. 63, 2016, pp. 263–286.

[7] Shirobokov, M., Trofimov, S., and Ovchinnikov, M., "Lunar Frozen Orbits for Small Satellite Communication/Navigation Constellations," Proceedings of the 72nd International Astronautical Congress, Dubai, UAE, October 25-29, 2021. Paper IAC-21.C1.4.6, 14 p.

[8] Folkner, W. M., Williams, J. G., Boggs, D. H., Park, R. S., and Kuchynka, P., "The Planetary and Lunar Ephemerides DE430 and DE431," Interplanetary Network Progress Report 42-196, 2014, 81 p.

[9] Petit, G. and Luzum, B., "IERS Conventions," IERS Technical Note 36, 2010, 179 p.

[10] Coffey, S. L., Deprit, A., and Deprit, E., "Frozen Orbits for Satellites Close to an Earth-Like Planet," *Celestial Mechanics and Dynamical Astronomy*, Vol. 59, No. 1, 1994, pp. 37–72.

[11] Kozai, Y., "Motion of a Lunar Orbiter," *Publications of the Astronomical Society of Japan*, Vol. 15, No. 3, 1963, pp. 301–312.

[12] Abad, A., Elipe, A., and Tresaco, E., "Analytical Model to Find Frozen Orbits for a Lunar Orbiter," *Journal of Guidance, Control, and Dynamics*, Vol. 32, No. 3, 2009, pp. 888–898.

[13] Nie, T. and Gurfil, P., "Lunar Frozen Orbits Revisited," *Celestial Mechanics and Dynamical Astronomy*, Vol. 130, 2018. Article 61, 35 p.

[14] Lara, M., Ferrer, S., and De Saedeleer, B., "Lunar Analytical Theory for Polar Orbits in a 50-Degree Zonal Model Plus Third-Body Effect," *The Journal of the Astronautical Sciences*, Vol. 57, No. 3, 2009, pp. 561–577.

[15] Lara, M., "Design of Long-Lifetime Lunar Orbits: A Hybrid Approach," *Acta Astronautica*, Vol. 69, No. 3–4, 2011, pp. 186–199.

[16] Folta, D. and Quinn, D., "Lunar Frozen Orbits," AIAA/AAS Astrodynamics Specialist Conference and Exhibit, Keystone, CO, August 21-24, 2006. Paper AIAA 2006-6749, 18 p.

[17] Gordienko, E. S., Ivashkin, V. V., and Simonov, A. V., "Analysis of Stability of Orbits of Artificial Lunar Satellites and Configuring of a Lunar Satellite Navigation System," *Solar System Research*, Vol. 51, No. 7, 2017, pp. 654–668.

[18] Elipe, A. and Lara, M., "Frozen Orbits About the Moon," *Journal of Guidance, Control, and Dynamics*, Vol. 26, No. 2, 2003, pp. 238–243.

[19] Russell, R. P. and Lara, M., "Long-Lifetime Lunar Repeat Ground Track Orbits," *Journal of Guidance, Control, and Dynamics*, Vol. 30, No. 4, 2007, pp. 982–993.

[20] Snoek, J., Larochelle, H., and Adams, R. P., "Practical Bayesian Optimization of Machine Learning Algorithms," Proceedings of the 26th Annual Conference on Neural Information Processing Systems (NeurIPS), Lake Tahoe, NV, December 3-8, 2012. 9 p.

[21] Nogueira, F., "Bayesian Optimization: Open source constrained global optimization tool for Python," software package v1.2.0 published online 16 May 2020 at https://github.com/fmfn/BayesianOptimization (retrieved 27 Aug 2022).

[22] Walker, J. G., "Some Circular Orbit Patterns Providing Continuous Whole Earth Coverage," *Journal of the British Interplanetary Society*, Vol. 24, 1971, pp. 369–384.

[23] Mozhaev, G. V., "The Problem of the Continuous Earth Coverage and the Kinematically Regular Satellite Networks, I," *Kosmicheskie Issledovaniya [Cosmic Research]*, Vol. 10, No. 6, 1972, pp. 833–840.

[24] Mozhaev, G. V., "The Problem of the Continuous Earth Coverage and the Kinematically Regular Satellite Networks, II," *Kosmicheskie Issledovaniya [Cosmic Research]*, Vol. 11, No. 1, 1973, pp. 59–69.

[25] Ballard, A. H., "Rosette Constellations of Earth Satellites," *IEEE Transactions on Aerospace and Electronic Systems*, Vol. AES-16, No. 5, 1980, pp. 656–673.

[26] Lee, S. and Mortari, D., "Quasi-Equal Area Subdivision Algorithm for Uniform Points on a Sphere with Application to Any Geographical Data Distribution," *Computers and Geosciences*, Vol. 103, 2017, pp. 142–151.

[27] Renault, C. A. and Scheeres, D. J., "Statistical Analysis of Control Maneuvers in Unstable Orbital Environments," *Journal of Guidance, Control, and Dynamics*, Vol. 26, No. 5, 2003, pp. 758–769.

[28] Gustafson, E. D. and Scheeres, D. J., "Optimal Timing of Control-Law Updates for Unstable Systems with Continuous Control," *Journal of Guidance, Control, and Dynamics*, Vol. 32, No. 3, 2009, pp. 878–887.

[29] Beckman, M. and Lamb, R., "Stationkeeping for the Lunar Reconnaissance Orbiter (LRO)," 20th International Symposium on Space Flight Dynamics (ISSFD), Annapolis, MD, September 24-28, 2007. Paper 18-3, 15 p.

[30] Sweetser, T. H., Wallace, M. S., Hatch, S. J., and Roncoli, R. B., "Design of an Extended Mission for GRAIL," AIAA/AAS Astrodynamics Specialist Conference, Minneapolis, MN, August 13-16, 2012. Paper AIAA 2012-4429, 19 p.